Hindawi
International Journal of Antennas and Propagation
Volume 2022, Article ID 9066614, 6 pages
https://doi.org/10.1155/2022/9066614

Research Article

Near-Field Electromagnetic Scatterings and Imaging of a Ship Based on High-Frequency Techniques

Conghui Qi,[1] **Wei Yang**,[2] **and Xiaozhang Zhu**[2]

[1]*School of Electrical Engineering and Electronic Information, Xihua University, Chengdu 610039, China*
[2]*School of Electronic Science and Engineering, University of Electronic Science and Technology of China, Chengdu 611731, China*

Correspondence should be addressed to Xiaozhang Zhu; xzzhu@uestc.edu.cn

Received 4 June 2021; Revised 20 April 2022; Accepted 13 August 2022; Published 9 September 2022

Academic Editor: Hervé Aubert

In radar detection, it is important to investigate the near-field scattering characteristics since the far-field condition is not easily satisfied for the distance between the radar and the electrically large ship on the sea surface. A high-frequency techniques of the physical optics (PO) and shooting and bouncing rays (SBR) with local expansions based on the facets of the target are proposed to take the electromagnetic scatterings in the near zone. Therefore, it is a more straightforward method to modify the computation from traditional far-field problem to near-field problem with the singularity-free characteristic. Simulation results show that it has high accuracy but requires very little increase in computational costs in the near-field problem. Moreover, the 1-D high-resolution range profile (HRRP) demonstrates that the near-field scattering mechanism is much different from the cases in the traditional far-field problem.

1. Introduction

The electromagnetic (EM) backscattering from a large target plays an important role in target detection and monitoring. However, in the ocean environment, the distance between the target and detecting radar is not far enough to satisfy the far-field condition for the target on the sea surface especially when the target is large. For example, for a ship with a length of 150 m at X band, its far-field distance is a minimum observation distance from the radar on the order of 1200 km [1, 2]. Actually, most previous studies of this kind of problem have simply considered as the scattering in the far-field problem [3]. However, the scattering characteristic in the near field is much different from the far field. Thus, the analysis of the near-field scattering is very necessary when the large target is in the near zone. Such a large target is more easily characterized by using high-frequency techniques from a computational perspective, such as the physical optics (PO) and shooting and bouncing rays (SBR) [4, 5]. Therefore, the near-field scattering of a ship model is well worth investigating by using high-frequency techniques.

To our knowledge, few studies are involved in the near-field analysis [6–8]. In the near-field calculation, the scattering calculation is generally formulated as a surface integral [9] of the assumed currents uniformly distributed on the divided facets. It is problematic since it requires fine meshing facets. Alternatively, Gordon [10] presented a contour-integral representation for the near-field mono-static problem, which requires coarse meshing facets with a lower computation complexity. Unfortunately, his final expression suffers from the singularity problem when the projected point of the near-field source falls right on the facet contour of the interesting target. Cui's valuable work [11] extends the Gordon's representation and presents a treatment to the singularity problem and to derive analogous contour-integral representations for both the electric and magnetic scattered fields. However, it is much complicated in the computation and only involves a mono-static scattering problem.

In this paper, the different order expanded phase approximations are investigated to characterize the scattering behaviour of phase term in Green's function in the near field. Then, the local expansion based on the facets of the target is presented to account the near-field scattering contributions into account since this expansion relies on a phase approximation of the same order as the one used in the standard formulation in the far field, which is a more straightforward

method to modify the computation from traditional far-field problem to near-field problem. Also, it is particularly attractive since the proposed method requires very little increase in computational cost and yields excellent accuracy in the near-field scattering computation. In order to investigate the difference between the near-field backscattering and the far-field backscattering, the one-dimensional (1-D) high-resolution range profile (HRRP) in the near zone is employed to provide deeper insights into the scatterings. In these simulations, the full-size ship at X band is employed here, which is such large scale that few researches have been involved.

2. Different-Order Phase Approximation

For source point r' and observation point$r$, the distance $R = |r - r'|$should be examined to develop the relationships between approximations and minimum distance requirements. The standard procedure of $|r - r'|$is to obtain the approximation by Taylor expansion [12]; thus,

$$\begin{aligned}\left|\mathbf{r}-\mathbf{r}'\right| &= r - \hat{\mathbf{r}}\bullet\mathbf{r}' + \frac{1}{2r}\left(\mathbf{r}'^{2} - \left(\hat{\mathbf{r}}\bullet\mathbf{r}'\right)^{2}\right) \\ &\quad + \frac{1}{2r^{2}}\left(\mathbf{r}'^{2}\hat{\mathbf{r}}\bullet\mathbf{r}' - \left(\hat{\mathbf{r}}\bullet\mathbf{r}'\right)^{3}\right) + O\left(\frac{1}{r^{3}}\right),\end{aligned} \tag{1}$$

where $\hat{\mathbf{r}}$ is the unit vector of $\mathbf{r}$.

The approximations of interest in (1), characterized by their order in $1/r$, are the zeroth-order approximation $R_0(\mathbf{r},\mathbf{r}')$ and the first-order approximation $R_1(\mathbf{r},\mathbf{r}')$. The number of terms retained, in accordance with the order, essentially dictates the accuracy of the expansion series.

The zeroth-order approximation $R_0(\mathbf{r},\mathbf{r}')$ and its dominant error term $\Delta_1(\mathbf{r},\mathbf{r}')$ of order $O(1/r)$are expressed as

$$R_0(\mathbf{r},\mathbf{r}') = r - \hat{\mathbf{r}}\bullet\mathbf{r}' \approx \left|\mathbf{r}-\mathbf{r}'\right|, \tag{2a}$$

$$\Delta_1(\mathbf{r},\mathbf{r}') = \frac{1}{2r}\left(\mathbf{r}'^{2} - \left(\hat{\mathbf{r}}\bullet\mathbf{r}'\right)^{2}\right). \tag{2b}$$

Therefore, the behaviour of the phase term in Green's function is $e^{-jk|\mathbf{r}-\mathbf{r}'|} \approx e^{-jkr}\bullet e^{jk\hat{\mathbf{r}}\bullet\mathbf{r}'}$.

Alternatively, the first-order approximation $R_1(\mathbf{r},\mathbf{r}')$ and its dominant error term $\Delta_2(\mathbf{r},\mathbf{r}')$of order $O_2(1/r)$ are expressed as

$$R_1(\mathbf{r},\mathbf{r}') = r - \hat{\mathbf{r}}\bullet\mathbf{r}' + \frac{1}{2r}\left(\mathbf{r}'^{2} - \left(\hat{\mathbf{r}}\bullet\mathbf{r}'\right)^{2}\right) \approx \left|\mathbf{r}-\mathbf{r}'\right|, \tag{3a}$$

$$\Delta_2(\mathbf{r},\mathbf{r}') = \frac{1}{2r^{2}}\left(\mathbf{r}'^{2}\hat{\mathbf{r}}\bullet\mathbf{r}' - \left(\hat{\mathbf{r}}\bullet\mathbf{r}'\right)^{3}\right). \tag{3b}$$

Therefore, the behaviour of the phase term in Green's function is $e^{-jk|\mathbf{r}-\mathbf{r}'|} \approx e^{-jkr}\bullet e^{jk\hat{\mathbf{r}}\bullet\mathbf{r}'}\bullet e^{-jk1/2r\left(\mathbf{r}'^{2}-\left(\hat{\mathbf{r}}\bullet\mathbf{r}'\right)^{2}\right)}$.

This phase expansion will inevitably lose accuracy for fixed r' and increasing r. This is illustrated in Figure 1 which depicts an observation point situated on the x axis at $(x, 0)$. This is illustrated in Figure 1 which depicts the phase error $\Delta\varphi$ between the exact phase term and approximation $R_0(\mathbf{r},\mathbf{r}')$ and $R_1(\mathbf{r},\mathbf{r}')$ at an observation point $(x, 0)$ situated on the x axis, respectively. The point sources are located at $(0, y)$ over a length $D = 133m$, reproducing the dimension of a surveillance ship and the electromagnetic wavelength $\lambda = 0.03m$ at $10GHz$.

Each point (x, y) in Figure 1 corresponds to the phase error of the source at $(0, y)$ when observed from the point $(x, 0)$. The phase error is shown to oscillate increasingly quickly between $-\pi$ to π as we move away from the center elements when using the traditional zeroth-order approximation in Figure 1(a), while the first-order approximation in Figure 1(b) produces a more accurate phase approximation. However, it should be clarified that the phase error for a ship target in the near-field zone will be much more complicated since it is an ensemble of phase errors from all source points. It is proved that the phase factor is an important issue in near-field scattering problem.

3. Near-Field High-Frequency Techniques

It is problematic since it relies on the high-order approximate Green's function in the calculation of near-field scattering. An alternative approach relying on a phase approximation of the same order as the one used in the standard formulation in the far field is here presented.

3.1. Local Expansions. The procedure for a large target is to subdivide its surface S into a collection of facets with each facet Sn, n = 1, 2, ⋯ N, and N is the facet number of target. For a source point r′ at a given n-th facet with its geometry center $\mathbf{r}'^{(n)}_{c}$, the phase term of Green's function can be expanded at a center $\mathbf{r}'^{(n)}_{c}$; thus, the standard procedure of $|\mathbf{r}-\mathbf{r}'|$is

$$\begin{aligned}\left|\mathbf{r}-\mathbf{r}'\right| &= \left|\mathbf{r}-\mathbf{r}'^{(n)}_{c} - \mathbf{r}' + \mathbf{r}'^{(n)}_{c}\right| \\ &\approx \left|\mathbf{r}-\mathbf{r}'^{(n)}_{c}\right| - \hat{\mathbf{k}}^{(n)}\left(\mathbf{r}' - \mathbf{r}'^{(n)}_{c}\right),\end{aligned} \tag{4}$$

where the unit vector $\hat{\mathbf{k}}^{(n)}$is defined by $\hat{\mathbf{k}}^{(n)} = (\mathbf{r}-\mathbf{r}'^{(n)}_{c})/|\mathbf{r}-\mathbf{r}'^{(n)}_{c}|$; $\mathbf{r}'$is on the n-th facet of target of interest. If $\mathbf{r}'^{(n)}_{c} = \mathbf{r}'_{0}$ is the geometry center of target, the above expression recovers to the original formulation in far-field problem.

On the contrary, $\mathbf{r}$ denotes the location of the transmitted radar or received radar. For the transmitted radar, $\mathbf{r} = \mathbf{r}_{\mathrm{i}}$, $\mathbf{r}_{\mathrm{i}} = -\mathrm{r}_{\mathrm{t}}\hat{\mathbf{r}}_{i}$; for the received radar, $\mathbf{r} = \mathbf{r}_{s}$, $\mathbf{r}_{s} = -\mathrm{r}_{r}\hat{\mathbf{r}}_{s}$. Here, r_{t}, $\hat{\mathbf{r}}_{i}$are the magnitude and direction of the vector from the position of transmitted radar to the geometry center of the target, respectively. Also, r_{r}, $\hat{\mathbf{r}}_{s}$ are the magnitude and direction of the vector from the geometry center of the target to position of transmitted radar, respectively. Therefore, the unit vector $\hat{\mathbf{k}}^{(n)}$ can be rewritten as [13]

(1) For the incident wave on n-th facet,

$$\hat{\mathbf{k}}^{(n)}_{\mathrm{i}} = \frac{\mathbf{r}'^{(n)}_{c} - \mathbf{r}_{\mathrm{i}}}{\left|\mathbf{r}'^{(n)}_{c} - \mathbf{r}_{\mathrm{i}}\right|}. \tag{5a}$$

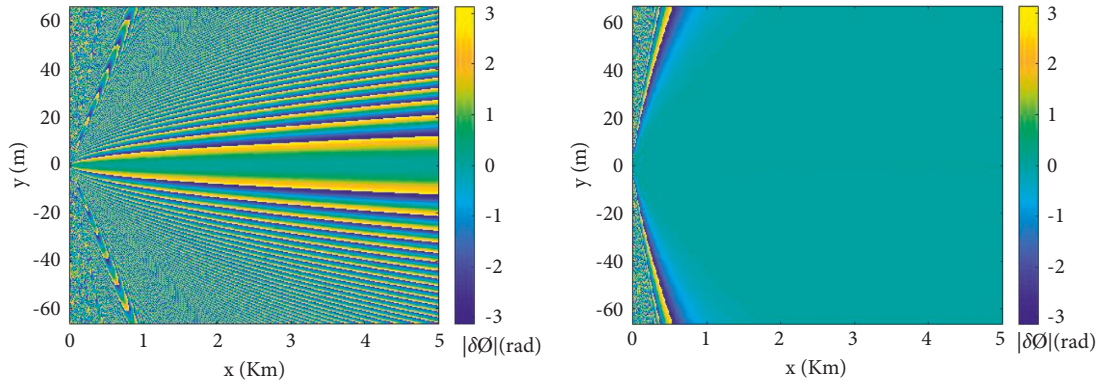

Figure 1: Comparisons on phase approximations. (a) Zeroth-order approximation. (b) First-order approximation.

(2) For the scattered wave from n-th facet,

$$\hat{\mathbf{k}}_s^{(n)} = \frac{\mathbf{r}_s - \mathbf{r}'^{(n)}_c}{\left|\mathbf{r}'^{(n)}_c - \mathbf{r}_s\right|}. \tag{5b}$$

3.2. Modifications of High-Frequency Techniques. Instead of the plane wave in the far-field problem, the spherical wave excited by a point source is represented as a primary illumination. According to the phase approximation based on the expansion center $\mathbf{r}'^{(n)}_c$ on n-th facet, thus, the incident electric field at $\mathbf{r}'$ is

$$\begin{aligned}\mathbf{E}_i^{(n)}(r') &= \frac{e^{-jk\left(|\mathbf{r}_i - \mathbf{r}'|\right)}}{\left|\mathbf{r}_i - \mathbf{r}'\right|} \bullet \hat{\mathbf{e}}_i \\ &\approx \frac{e^{-jk\left(|\mathbf{r}_i - \mathbf{r}'^{(n)}_c|\right)} e^{-jk\hat{\mathbf{k}}_i^{(n)} \bullet \left(\mathbf{r}' - \mathbf{r}'^{(n)}_c\right)}}{\left|\mathbf{r}_i - \mathbf{r}'^{(n)}_c\right|} \bullet \hat{\mathbf{e}}_i,\end{aligned} \tag{6}$$

where $\hat{\mathbf{e}}_i$denotes the polarization vector of incident electric field, the wavenumber $k = 2\pi/\lambda$.

Consistent with the assumptions for far-field illumination and observation, the above approximation applies to both primary illumination for physical optics (PO) method and electromagnetic secondary interaction effect for shooting and bouncing ray (SBR) method. For the SBR computation, its unit vector of incident wave and incident field is determined by equations (5a) and (6), respectively, replacing the plane wave in far-field problem [14].

For the PO calculation, since the quantity $\hat{\mathbf{r}}_s$ is now insufficiently accurate, it should be replaced by the $\hat{\mathbf{k}}_s^{(n)}$. Also, the counterparts to the standard integral representations are straightforwardly obtained by modifying the quantity $\kappa = \hat{\mathbf{r}}_i - \hat{\mathbf{r}}_s$ to $\kappa^{(n)} = \hat{\mathbf{k}}_i^{(n)} - \hat{\mathbf{k}}_s^{(n)}$, as defining the $\hat{\mathbf{k}}_i^{(n)}, \hat{\mathbf{k}}_s^{(n)}$ in (5a). The scattered field by the primary illumination is then obtained by summing the contributions from all illuminated facets. Besides, the secondary scattered field by the interaction effect among the facets can be obtained by summing the contributions from all tracing ray tubes, where its scattered wave vector is determined by equation (5b). Thus, the total fields from primary and secondary contributions are coherently summed again.

Finally, the high-frequency technique and ray-tracing process are realized on graphics processing unit (GPU) where the algorithm is performed and accelerated in parallel [15, 16]. Therefore, the RCS simulator can be straightforwardly developed by modify the far-field computation based on the abovementioned treatments. For the computational cost, it is noted that the above treatments are only the modifications to the formulations in traditional far-field problem, and the proposed method requires very little increase in computational cost.

4. Simulation Results

Some simulations are investigated for the computation accuracy and scattering characteristics by using the proposed method.

4.1. Square Plate. For the computation accuracy, a 2 m square plate illuminated by a y-oriented electric Hertzian dipole with the moment $\alpha = 1$Am is employed to test the accuracy of the contour-integral representation based on the local expansion in the PO calculation. The dipole source is along a $r_i = 1.5$m arc that is directly above one of the plate's edges with elevation angle uniformly ranging from 0° to 90° with 0.25° step in the xz-plane. There are three different methods: standard surface integral [9], contour integral of Gordon's work [10], and the proposed method. Figure 2 shows that the proposed method has a quite good agreement compared to the standard surface integral. It has the singularity-free characteristic. In comparison, the singularity will appear along an entire segment of the arc by using the contour integral of Gordon's work. Therefore, it has been proved that the local expansion representation can solve the singularity problem of contour integral and provide a numerically stable result.

For the computation efficiency, Table 1 compares the number of meshing facets and computation time between the surface and contour integrals for this case. The meshing size of surface integral is much smaller than that of contour

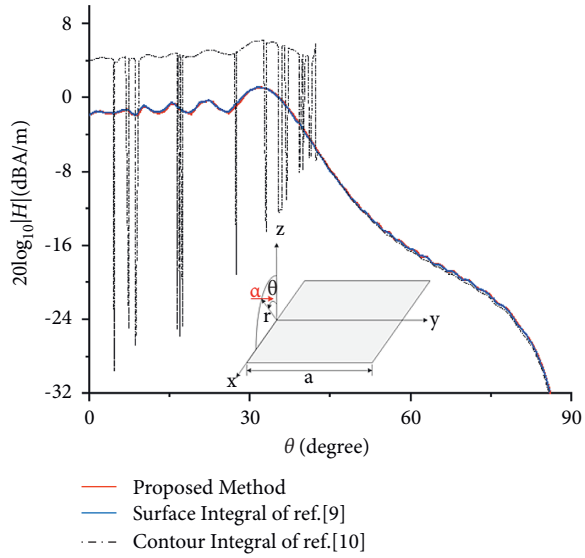

Figure 2: Scattering comparison by the local expansion.

Table 1: Comparison of computation complexity between contour and surface integrals.

	Meshing facets	Averaged computation time per angle (sec.)
Surface integral of ref. [9]	92140	2.45
The proposed method	216	0.12

integral. The ratio of computation complexity to calculate contour and surface integrals is about 1 : 426, and the ratio of the averaged computation time is more than 1 : 12 for each incident angle. Reduction in computational time is not the order of computation complexity since computation is in parallel in GPU acceleration. It indicates that the proposed method is more efficient for the scattering problem of an electrically large target.

4.2. Surveillance Ship. A surveillance ship is further investigated in the simulation, and the size is 132.8m (L) × 20m (W) × 23.3m (H), as shown in Figure 3. The radar frequency is at *X* band, 10GHz. In this condition, the far-field criterion is R ≥ 1200Km.

In near-field scattering, the radar distance R is a variable in the generalized RCS definition. The special scenario, such as the missile-target encounter scenario, is first investigated to analyze the complicated scattering phenomenon in the near field. The mono-static generalized radar cross section (σ_{nf}) [17] of horizontal-horizontal (HH) and vertical-vertical (VV) polarization scatterings of the ship is also investigated to analyze the scattering differences between the traditional far field and the near field, at different distances 1km and 10km. The radar incident angles are of the azimuthal angles$\Phi = 0^\circ \sim 180^\circ$, at a supposed elevation$\Phi = 75^\circ$.

As shown in Figure 4, the near-field scatterings are obviously different from the far-field results. Also, there are some interesting scattering phenomena that the near-field

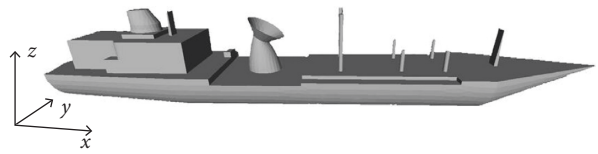

Figure 3: A surveillance ship.

scattering values are much smaller than far-field scattering at three azimuth angles $\Phi = 0^\circ; 90^\circ; 180^\circ$. It can be explained that the scattering from some dihedral structures composed of deck and ship's emplacement has significant scattering contributions in far-field problem, but the near-field scatterings fail. In the far field, the EM reflected rays will go back to the direction of incidence, resulting in a larger mono-static scattering, but the EM rays cannot return to the original direction in the near-field problem due to the divergences of the incident wave.

Furthermore, in order to explore the scattering mechanisms in the near zone, the one-dimensional (1-D) high-resolution range profile (HRRP) [18] is employed to provide deeper insights into the scatterings, as shown in Figure 5. The resolution is 0.5m, and its radar bandwidth is B = 300MHz at a central frequency f_{c0} = 10GHz. Each point scatterer is associated with the effective scattering of its nearby subregion. Some scatterings do have not a distinct contribution in short radar distances, even some scattering characteristics disappear. In contrast, the scatterings of the plane region become stronger. It indicates that the near-field

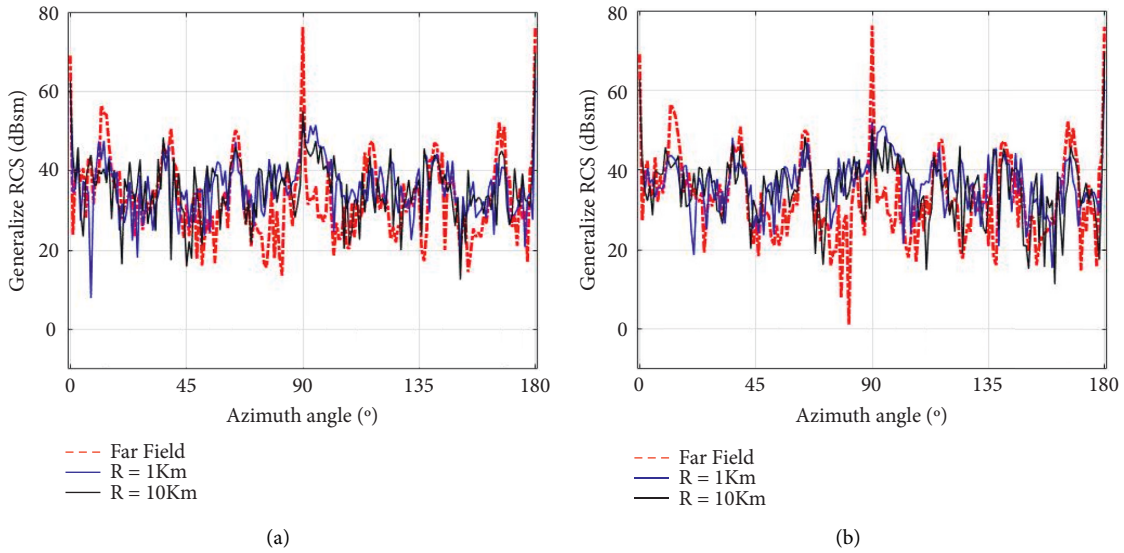

Figure 4: Scattering differences between far field and near field. (a) HH polarization. (b) VV polarization.

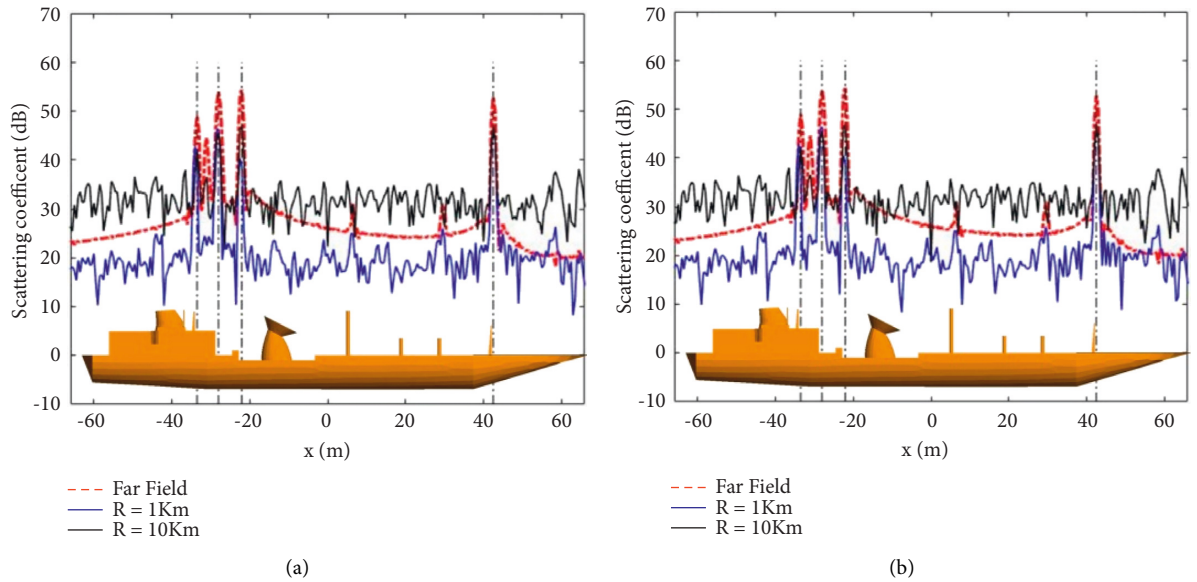

Figure 5: High-resolution range profile (HRRP) at different distances. (a) HH polarization. (b) VV polarization.

scattering energy is divergent and nondirectional, which leads to a more complicated scattering problem.

5. Conclusion

For an electrically large target, the far-field distance in electromagnetic scattering is hard to be satisfied in real radar target detection systems. Thus, the near-field scattering analysis is an urgent problem in order to investigate the ship backscattering characteristic. The scattering computation of a ship target in the near zone is implemented by the high-frequency techniques with some modifications in formulations. It indicates that the proposed method with the local expansions based on the facets of the target has an excellent accuracy without an increase in computational cost. From the simulation results, it is found that the near-field scattering is quite different from the far-field problem. It is also noted that the near-field scattering is a comprehensive problem, involving the radar parameters, frequency, distance, incident angle, etc., and the radar antenna pattern. Therefore, more workers are needed in this research area.

Data Availability

The data used to support the findings of this study are available from the corresponding author upon request.

Conflicts of Interest

The authors declare that they have no conflicts of interest.

Acknowledgments

This work was supported by the National Natural Science Foundations for Young Scholars of China (61901394 and 61801090) and Sichuan Science and Technology Program (2022NSFSC0909 and 2022NSFSC0490).

References

[1] S. R. Legault, "Refining physical optics for near-field computations," *Electronics Letters*, vol. 40, no. 1, pp. 71-72, 2004.

[2] C. L. Dong, L. X. Guo, X. Meng, and X. Meng, "An accelerated algorithm based on go-po/ptd and cwmfsm for em scattering from the ship over a sea surface and sar image formation," *IEEE Transactions on Antennas and Propagation*, vol. 68, no. 5, pp. 3934–3944, 2020.

[3] J. W. Hao and X. Q. Sheng, "Accurate and efficient simulation model for the scattering from a ship on a sea-like surface," *IEEE Geoscience and Remote Sensing Letters*, vol. 14, no. 12, pp. 2375–2379, 2017.

[4] W. F. Huang, Z. Zhao, R. Zhao, J. Y. Wang, Z. Nie, and Q. H. Liu, "GO/PO and PTD with virtual divergence factor for fast analysis of scattering from concave complex targets," *IEEE Transactions on Antennas and Propagation*, vol. 63, no. 5, pp. 2170–2179, 2015.

[5] R. Wang, G. B. Guo, Z. Y. He, and L. X. Guo, "Scattering prediction of target above layered rough surface based on time-domain ray tracing modeling," *IEEE Transactions on Antennas and Propagation*, vol. 69, no. 5, pp. 2820–2832, 2021.

[6] G. B. Guo and L. X. Guo, "SBR method for near-field scattering of an electrically large complex target illuminated by dipole sources," *IEEE Access*, vol. 6, pp. 78710–78718, 2018.

[7] H.-T. Chou, W.-J. Gao, J. Zhou, B. You, and X.-H. He, "Enhancing electromagnetic backscattering responses for target detection in the near zone of near-field-focused phased array antennas," *IEEE Transactions on Antennas and Propagation*, vol. 69, no. 3, pp. 1658–1669, 2021.

[8] B. Chen and C. M. Tong, "Near-field scattering prediction based on refined time-domain high-frequency method," *IEEE Antennas and Wireless Propagation Letters*, vol. 18, no. 6, pp. 1194–1198, 2019.

[9] R. Deban, H. Boutayeb, K. Wu, and J. Conan, "Deterministic approach for spatial diversity analysis of radar systems using near-field radar cross section of a metallic plate," *IEEE Transactions on Antennas and Propagation*, vol. 58, no. 3, pp. 908–916, 2010.

[10] W. B. Gordon, "Contour integral representation for near field backscatter from a flat plate," *IEEE Transactions on Antennas and Propagation*, vol. 60, no. 5, pp. 2587–2589, Mar, 2012.

[11] T. T. Fan, X. Zhou, and T. J. Cui, "Singularity-free contour-integral representations for physical-optics near-field backscattering problem," *IEEE Transactions on Antennas and Propagation*, vol. 65, no. 2, pp. 805–811, 2017.

[12] A. Gendelman, Y. Brick, and A. Boag, "Multilevel physical optics algorithm for near field scattering," *IEEE Transactions on Antennas and Propagation*, vol. 62, no. 8, pp. 4325–4335, 2014.

[13] C. H. Qi, Y. Yi, and W. Yang, "An efficient high-frequency method of the EM near-field scattering from an electrically large target," *Frequenz*, vol. 75, no. 11-12, pp. 487–492, 2021.

[14] W. Yang, C. J. Liao, X. Z. Zhu, C. H. Qi, S. W. Lei, and H. Q. Hu, "An effective high-frequency method for the near-field scattering from an electrically large ship illuminated by a hertzian dipole," *IEEE Geoscience and Remote Sensing Letters*, vol. 19, pp. 1–5, 2022.

[15] W. Yang, C. Y. Kee, and C. F. Wang, "Novel extension of SBR-PO method for solving electrically large and complex electromagnetic scattering problem in half-space," *IEEE Transactions on Geoscience and Remote Sensing*, vol. 55, no. 7, pp. 3931–3940, 2017.

[16] L. Linghu, J. Wu, Z. Wu, G. Jeon, and X. Wang, "GPU-accelerated computation of time-evolving electromagnetic backscattering field from large dynamic sea surfaces," *IEEE Transactions on Industrial Informatics*, vol. 16, no. 5, pp. 3187–3197, 2020.

[17] W. Yang, C. J. Liao, and H. Q. Hu, "Analysis on near-field electromagnetic scattering of a ship on sea surface based on high-frequency technique," *IEEE International Conference on Consumer Electronics*, vol. 63, pp. 52-53, 2020.

[18] C. Ozdemir, *Inverse Synthetic Aperture Radar Imaging with MATLAB Algorithms*, Wiley, 2012.